

High-pressure torsion of thick Cu and Al–Mg–Sc ring samples

Hideaki Iwaoka^{1,2} · Zenji Horita^{1,2}

Received: 28 January 2015 / Accepted: 16 April 2015 / Published online: 24 April 2015
© Springer Science+Business Media New York 2015

Abstract Pure Cu and an Al–3 %Mg–0.2 %Sc alloy are processed by high-pressure torsion with ring-shape samples having an initial thickness of 4 mm. Microstructural observation across the thickness is carried out using optical microscopy and transmission electron microscopy to correlate with hardness variation. It is shown that the strain is introduced more intensely in the center of thickness on the cross sections for both pure Cu and the Al alloy. This area expands with an increasing number of revolutions but the expansion saturates before covering the entire cross section. Softening occurs with straining in pure Cu but saturation reaches without softening in the Al alloy. It is suggested that imposed strain is estimated using the thickness of severely deformed region.

Introduction

It is well known that torsional straining under high pressures, so-called high-pressure torsion (HPT) [1], is effective to produce ultrafine grains in metallic materials [2–4]. It is applicable to hard and less ductile materials [5, 6] even to intermetallics [7–9], ceramics [10–13], and semiconductors [14–17]. The samples for the HPT are used in the form of disk or ring and [18, 19], because the shear strain is

introduced in proportion to the distance from the rotation center [1], the ring sample is preferable to achieve a homogeneous structure throughout the sample [18, 19]. The magnitude of the shear strain is also determined by the sample thickness: thinner the sample, more the shear strain is introduced as the shear strain is inversely proportional to the thickness [1].

For the HPT processing, the sample is usually used in disk shape with the thickness less than 1 mm but a few studies were attempted on thicker samples [20–27]. By changing the ratio of the thickness to the diameter of the disk, Hohenwarter et al. [22] examined the effect of the thickness on the microstructural homogeneity and reported that there was a thickness limitation for achieving homogeneous microstructure throughout the thickness direction. Sakai et al. [20] used cylindrical samples with the height almost similar to the diameter but reported that the strain was rather centered around the cylinder height, although this heterogeneity was less significant using an incremental HPT process recently developed by Hohenwarter [27]. The present authors adopted ring samples for HPT processing [23, 24] but the strain was preferentially introduced at the thickness center and the microstructural homogeneity was not established when the sample thickness is thicker. It appears that the microstructural heterogeneity is not due to the sample types (i.e., disk or ring). This earlier study employed pure Al which is known to exhibit softening with intense straining because dynamic recovery is more pronounced due to its high stacking fault energy [28–31]. In this study, pure Cu and the Al alloys are used because both materials did not show softening with intense straining but reach directly to saturation [19, 32]. Thus, this study aims to investigate the effect of materials on the homogeneity in the thick samples for the HPT processing.

✉ Hideaki Iwaoka
iwaoka@zaiko6.zaiko.kyushu-u.ac.jp

¹ Department of Materials Science and Engineering, Faculty of Engineering, Kyushu University, Fukuoka 819-0395, Japan

² WPI-International Institute for Carbon-Neutral Energy Research, Kyushu University, Fukuoka 819-0395, Japan

Experimental procedures

High-purity Cu (99.99 %) and an Al–3 %Mg–0.2 %Sc alloy were used with a ring shape for the HPT samples. The samples having outer and inner diameters of 20 and 14 mm with a thickness of 4 mm were cut from cold-rolled plates using an electrical discharge machine. To exclude any strain during compression before initiating rotation in the HPT processing, the ring samples were removed from the anvil after compression and subjected to annealing at 873 K for 1 h in both materials followed by cooling in the furnace for the pure Cu and quenched in cold water for the Al alloy. The ring samples were processed by HPT under a pressure of 2 GPa with a rotation speed of 0.5 rpm for revolutions of 1/8, 1/4, 1/2, 1, 5, 10, 30, and 50 for the Cu samples and of 1/4, 1/2, and 1 for the Al alloy samples.

Microstructures after the HPT processing were observed by optical microscopy (OM) using a Nikon ECLIPSE ME600 on the cross section illustrated in Fig. 1. The cross sections for the OM were first polished to mirror-like surfaces by emery papers and cloths containing an alumina suspension, and they were subjected to electropolishing using a solution of 10 %HClO₄–20 %C₃H₅(OH)₃–70 %C₂H₅OH for the pure Cu and 5 %HNO₃–25 %C₃H₅(OH)₃–70 %C₂H₅OH for the Al alloy. They were complimented with an aqueous solution of 50 %HNO₃ and a Barker’s reagent for revealing grain boundaries.

Vickers microhardness was measured on the same cross sections with mirror-like surfaces as prepared for OM. A load of 200 g was applied for duration of 15 s using an Akashi MVK-E3 testing machine. Figure 1 shows positions of the hardness measurements at the cross marks on the cross sections.

Results

Pure Cu

Figure 2 shows OM images of the Cu samples after processing by HPT. Dark contrast areas appear at the thickness center after $N = 1/8$ and they are replaced by bright contrast areas at the thickness center, while the dark contrast areas remain at the outward edges of the bright contrast areas and finally become invisible with the increasing number of the revolutions. Areas of coarse grains exist at outer edges of the cross sections and, although their fractions become smaller, they are retained even after $N = 50$. Figure 3 plots the change in the bright contrast width against the number of revolutions. This plot indicates that the width of the bright contrast continuously increases but the increase becomes gradual after $N = 10$ and appears to saturate to the total width of ~ 2 mm.

Figures 4 and 5 show TEM micrographs including selected area electron diffraction (SAED) patterns of the samples after $N = 1/4$ and 10 revolutions, respectively. The average grain size was measured to be 520 and 480 nm, respectively, from the dark-field images on the right. The microstructure after $N = 1/4$ consists of sub-grains with grain boundaries ill-defined, whereas the grain boundaries after $N = 10$ are well defined. The evolution of the microstructure is also recognized from the difference in the SAED patterns: diffracted beams form a net after 1/4 revolution but they are scattered around rings. These features suggest that the grain-boundary misorientation increases to be higher with straining in consistent with earlier reports [28].

The results of the hardness measurements are shown in Fig. 6, where the magnitude of hardness is color-coded according to the color scale as in the inset of the right-side

Fig. 1 Directions of observations by OM and TEM, and positions of hardness measurement

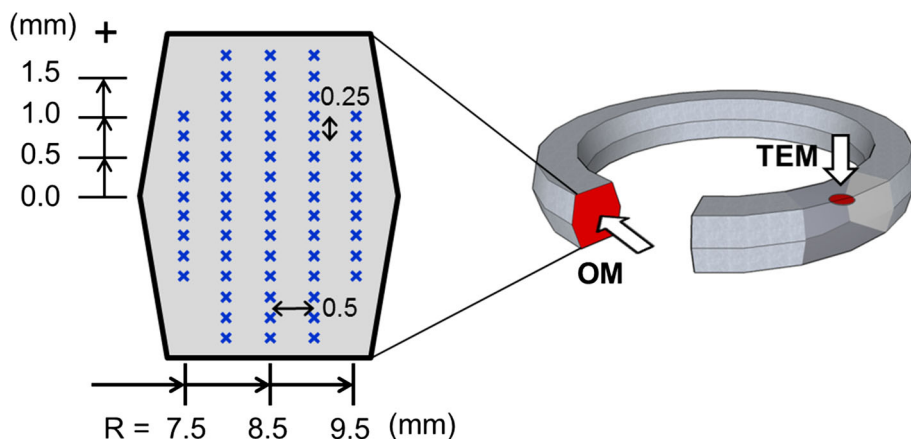
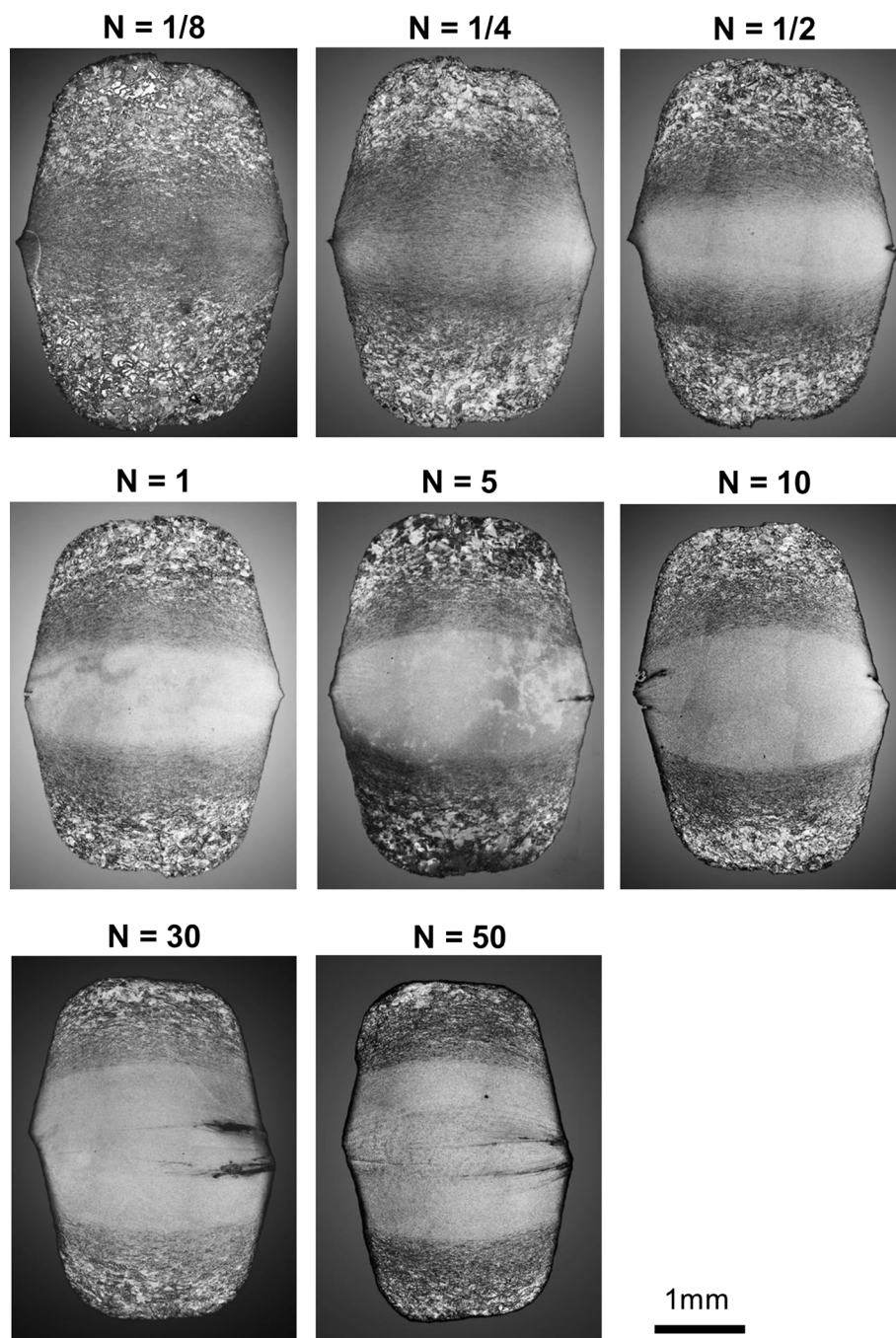


Fig. 2 Cross-sectional images of Cu rings observed by OM



bottom. The hardness at the thickness center is higher than those at the upper and lower parts on the cross section. The thickness center for the $N = 1/4$ sample has the highest hardness but those of the samples processed for more than $N = 1/2$ exhibit the hardnesses slightly lower than the ones in the neighboring areas. Such lower hardness areas expand toward the edges along the thickness direction with the increasing number of revolutions. This trend is consistent with the expanding behavior of the bright contrast area, and thus it is suggested that the areas with the bright contrast

correspond to the slight softer areas and those of the dark contrast areas to the higher hardness areas as shown in the OM observation of Fig. 2. This decrease in hardness should be due to the decrease in dislocation density.

Figure 7 shows the hardness variation along the thickness direction at the width center. The softening at the thickness center is clearly demonstrated in Fig. 7 with the decrease in hardness by up to 10 Hv. This trend is similar to the hardness change observed in pure Al [18, 28], although the fraction of the decrease is rather small as

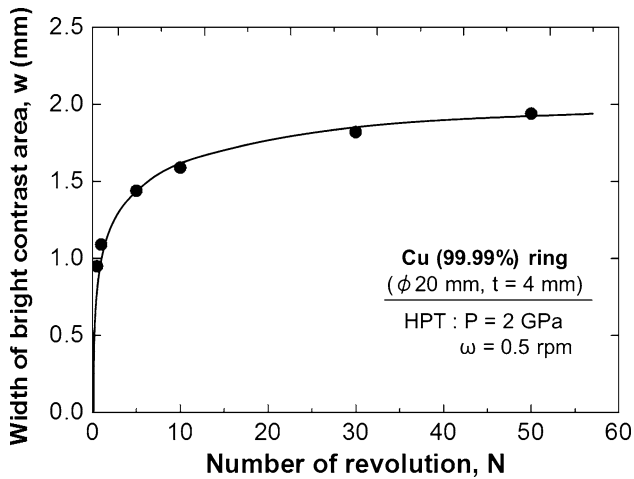


Fig. 3 Widths of bright contrast areas of Cu rings plotted against number of revolution

~8 % in pure Cu when compared with ~20 % in pure Al. An earlier measurement of hardness in HPT-processed pure Cu showed that the hardness increases and saturates to a constant level without taking a hardness maximum. Thus, the hardness variations observed in this study are conflict with the hardness measurements reported earlier on pure Cu [32]. It is considered that a temperature rise may be significant during the HPT processing because the thickness is thicker in the present study. This is also consistent with the grain size of ~520 nm which is bigger than reported earlier using thin disk samples where the grain size is ~200 nm.

Al–Mg–Sc alloy

Figure 8 shows OM images of the Al–Mg–Sc alloy after processing by HPT for (a) $N = 1/4$, (b) $N = 1/2$, and

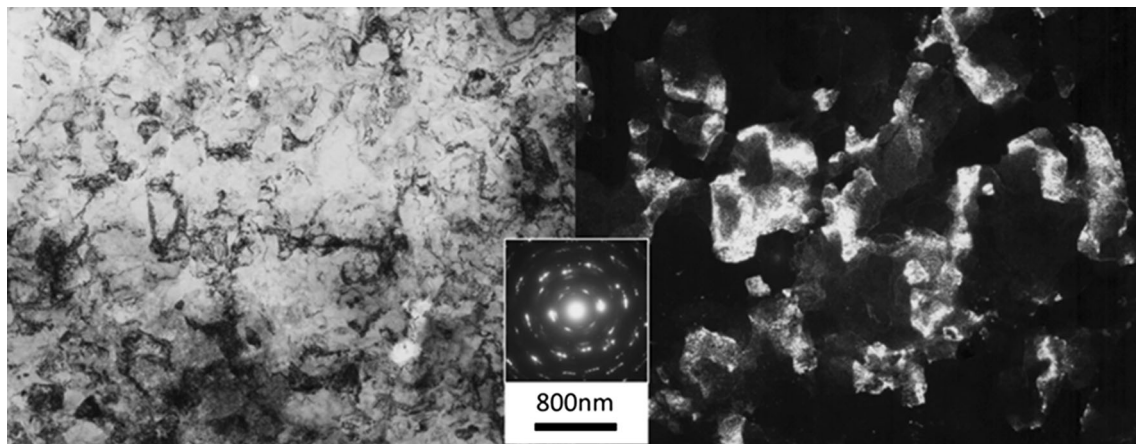


Fig. 4 TEM bright-field image (left) and dark-field image (right) with SAED pattern (inset) at thickness center of Cu after processing for $N = 1/4$

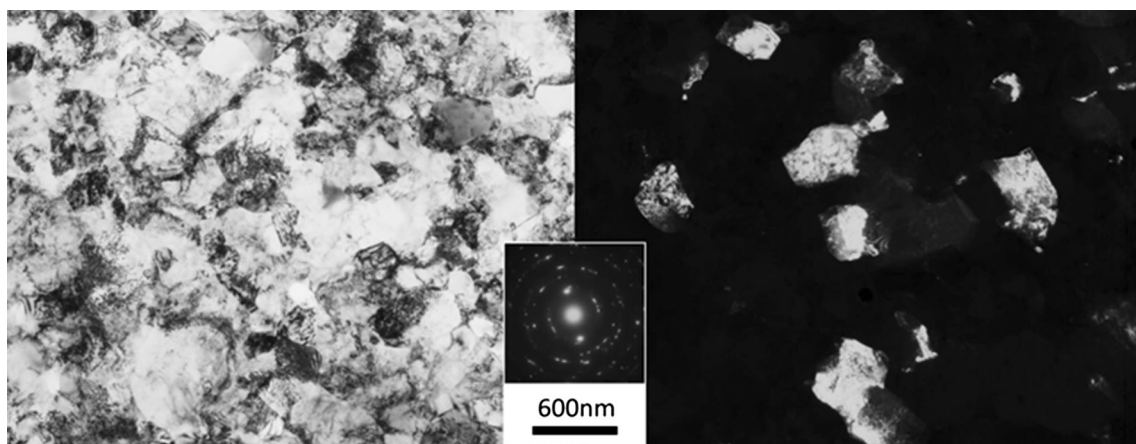


Fig. 5 TEM bright-field image (left) and dark-field image (right) with SAED pattern (inset) at thickness center of Cu after processing for $N = 10$

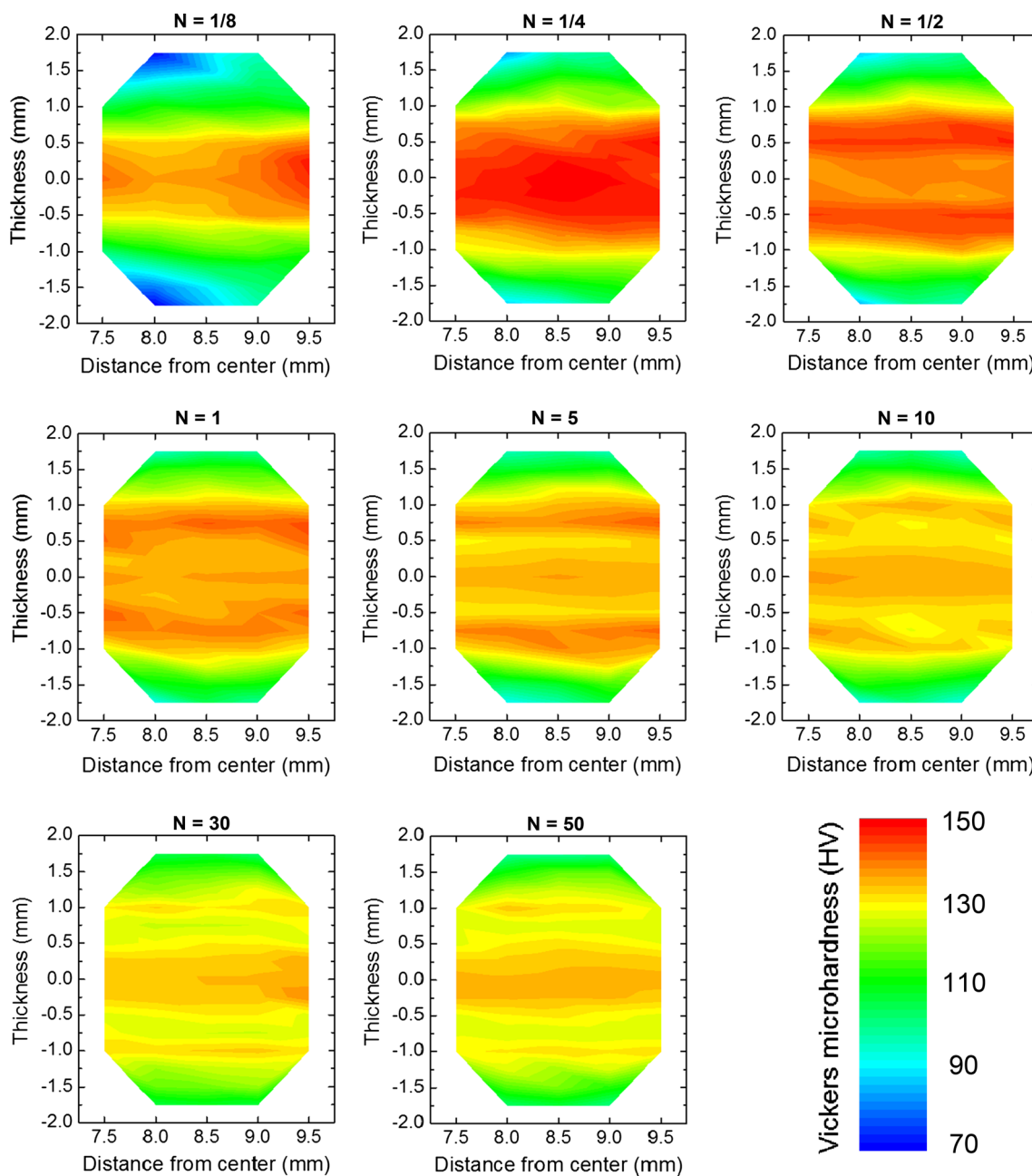


Fig. 6 Vickers microhardness on cross section of Cu rings color-coded according to color scale (Color figure online)

(c) $N = 1$ revolutions. A dark contrast area appears at the thickness center and its width expands along the thickness direction with the increasing number of revolution. However, the dark contrast area fails to cover the whole cross section as for the bright contrast area of pure Cu described above and for the dark contrast area of pure Al reported earlier [23, 24]. Coarse grain areas are visible both in the upper and lower parts on the cross section and remain unvarnished as the pure Cu of this study and the pure Al reported earlier [23, 24]. Figure 9 plots the maximum width of the dark contrast area against the number of

revolution. The width saturates after almost $N = 1/2$ and this saturation reaches quickly when compared with the case of pure Cu shown in Fig. 3, although the saturated level for the width seems fairly the same for both materials (~ 2 mm). It should be noted that the ring sample of the Al–Mg–Sc alloy broke at the thickness center into the upper and lower halves when the HPT processing was attempted for more than 1 revolution. This suggests that the hardening was very intense in the Al–Mg–Sc alloy.

TEM micrographs of the Al–Mg–Sc alloy after $N = 1$ are shown in Fig. 10 with a bright-field image on the left, a

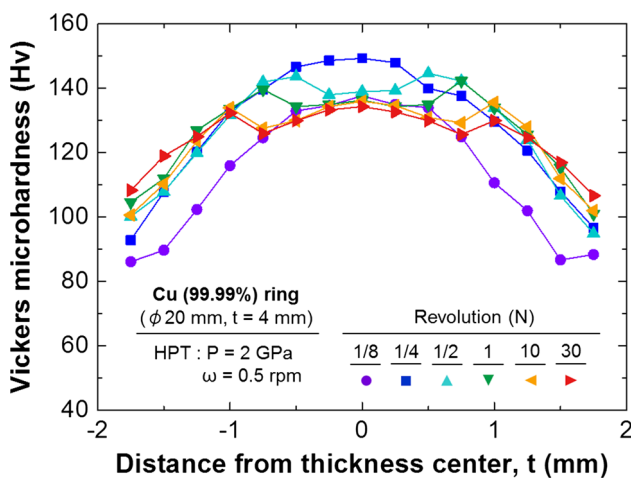


Fig. 7 Plots of Vickers microhardness along thickness direction at width center of pure Cu rings after HPT processing

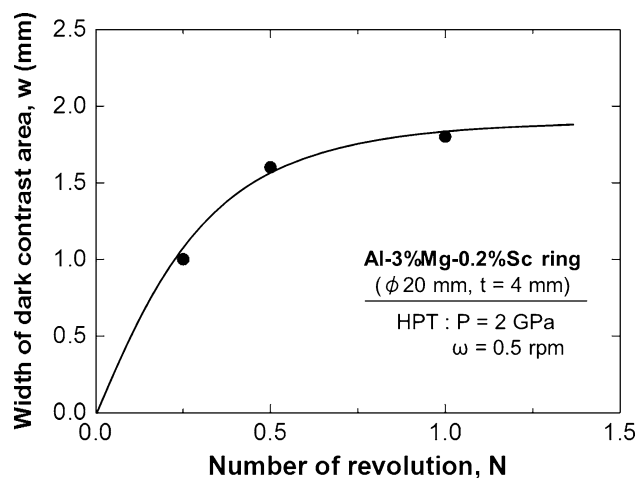


Fig. 9 Width of dark contrast area against number of revolution in Al–Mg–Sc rings

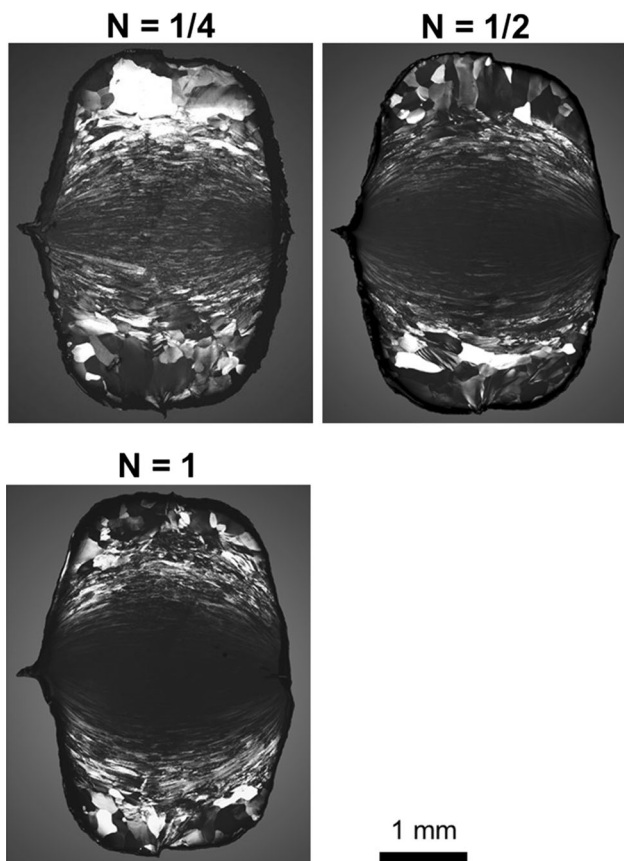


Fig. 8 Cross-sectional images of Al–Mg–Sc rings observed by OM

dark-field image on the right, and an SAED pattern as an inset. The observation was made at the thickness center with the dark contrast. The grain size appears to be ~200 nm and this grain size is similar to 150–230 nm obtained earlier after processing of thin disk and ring samples by HPT [19, 33, 34].

The hardness variation throughout the cross section of the Al–Mg–Sc alloy processed by HPT is shown in Fig. 11 for $N = 1/4, 1/2,$ and 1. The hardness at the thickness center is highest and it decreases toward the upper and lower edges for all numbers of revolutions. Thus, the area of higher hardness corresponds to the dark contrast area and this higher hardness area expands along the thickness direction. This hardness change appears to be consistent with the expanding behavior of the dark contrast shown in Fig. 8. Figure 12 confirms this hardness variation along the thickness direction, having a hardness maximum at the thickness center for each number of revolutions. The hardness decreases monotonically toward the upper and lower edges and this trend is different from the hardness variation observed in pure Cu shown in Fig. 7 and that in pure Al reported earlier [24].

Discussion

Softening with HPT processing was reported not only in pure Al but also in metals and alloys with low melting temperatures [18, 28–30, 35–38]. It was shown that this softening occurs dynamically during the HPT processing [39]. Because Cu has a higher melting temperature, softening was not observed during processing at room temperature but it does occur when it was processed at elevated temperature equivalent to room temperature of pure Al [40]. However, softening occurred in this study in pure Cu and it is considered that this is due to temperature rise during HPT processing because the sample thickness is thick in this study. It is likely that the heat generated in the thick sample by plastic deformation during HPT processing is less released through the anvils because of the reduction in contacting area of the sample surface with respect to the sample volume.

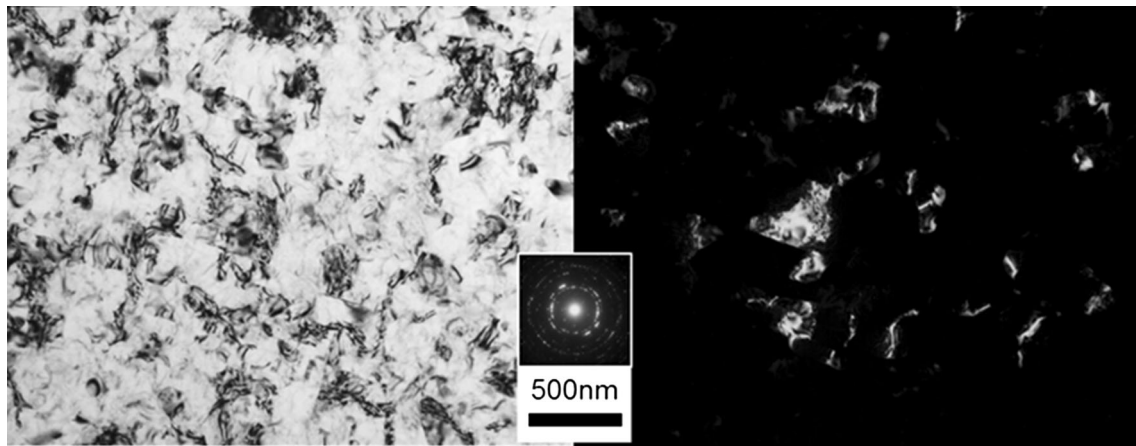


Fig. 10 TEM bright-field image (*left*) and dark-field image (*right*) with SAED pattern (*inset*) at thickness center of Al–Mg–Sc ring after processing for $N = 1$

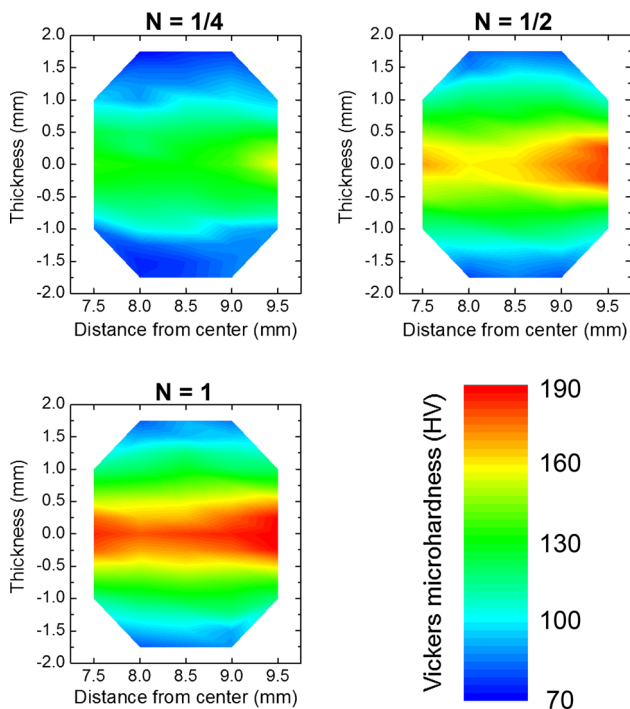


Fig. 11 Vickers microhardness on cross section of Al–Mg–Sc rings color-coded according to color scale (Color figure online)

This study has shown that, when the thickness is increased, the strain is introduced heterogeneously on the cross section: more at the thickness center but little at both upper and lower edges. The width of the well-strained regions is ~ 2 mm for both pure Cu and the Al alloy. This width remains almost the same even if the revolution for HPT is increased. Therefore, homogeneous structure over the entire cross section may be obtained if the sample thickness is less than 2 mm. The ratio of this thickness to the outer diameter ($2 \text{ mm}/\phi 20 \text{ mm}$) is very

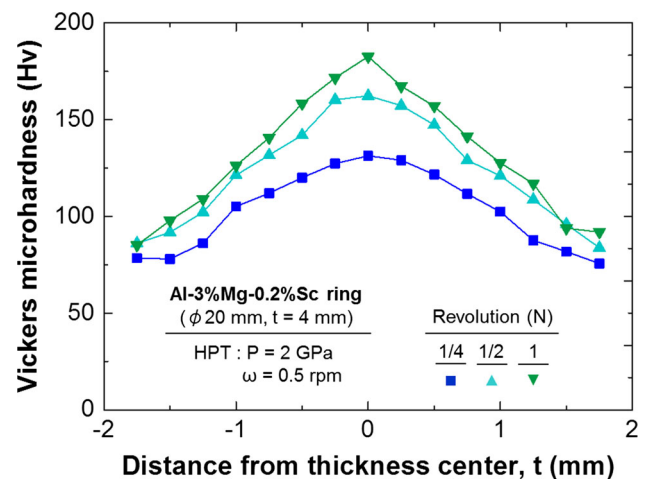


Fig. 12 Plots of Vickers microhardness along thickness direction at width center of Al–Mg–Sc rings after HPT processing

similar to the ratio in the case of disk sample reported by Hohenwarter et al. [22]. They used Armco iron disks having various ratios of the thickness to the diameter and concluded that the optimal ratio for obtaining homogeneous microstructure is $\sim 1/13$ or smaller. Additionally, in our previous study, we used high-purity Al ring samples having the outer and inner diameters of 30 and 24 mm with a thickness of 4 mm [23, 24]. Width of strained region saturated to slightly less than 3 mm and the ratio of this width to outer diameter ($3 \text{ mm}/\phi 30 \text{ mm}$) is again similar. These results indicate that the optimal ratio for achieving homogeneous microstructure depends neither on the sample shape (i.e., disk or ring) nor on the type of metals (i.e., softening occurs or not during HPT processing).

It may be important to estimate how much strain is introduced in the sample. The following equation is usually

used to calculate the equivalent strain ϵ produced by HPT processing [1, 41].

$$\epsilon = 2\pi rN/t, \tag{1}$$

where r is the distance from the rotation center, N is the number of revolution, and t is the sample thickness. Because the strained region is concentrated around the thickness center for thicker sample as in this study, it is obvious that t in Eq. (1) is no longer useful for the estimation of the strain. An earlier study by Harai et al. showed that the hardness increases monotonically with respect to the equivalent strain in the Al–Mg–Sc alloy. For this purpose, an additional experiment was conducted using a disk sample with a thin thickness (~ 0.65 mm) where the straining occurs throughout the thickness. The results are plotted in Fig. 13. Now, this plot can provide a unique relation between the hardness and the equivalent strain as in the study by Harai et al. [19].

Thus, the equivalent strain at the thickness center may be estimated from the hardness given in Fig. 13. The hardness and the corresponding equivalent strain are documented in Table 1 together with the thickness estimated through Eq. (1). Positions corresponding to the thickness are marked in Fig. 14 of the OM image shown in Fig. 8. It can be seen that the thickness calculated from equation using experimental strain is well consistent with thickness of intensely strained region observed in the OM image. This estimation suggests that the equivalent strain in thick sample imparted by HPT processing can be approximated through Eq. (1) with use of the thickness at the intensely strained region instead of using the thickness of the sample.

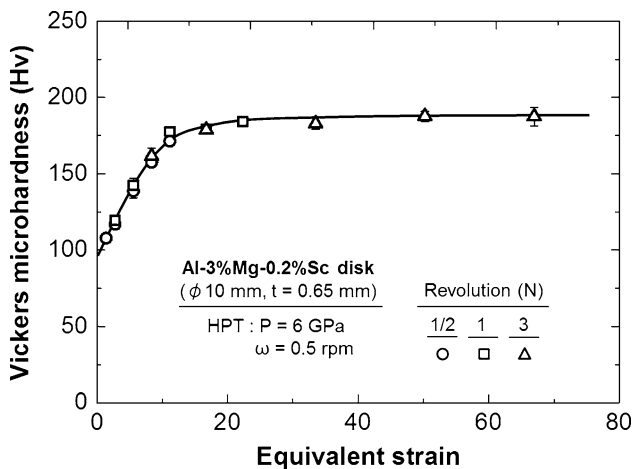


Fig. 13 Vickers microhardness plotted against equivalent strain after HPT processing of Al–Mg–Sc thin disk samples with thickness of ~ 0.65 mm

Table 1 Summary of equivalent strain at thickness center estimated from Fig. 13 and thickness calculated through Eq. (1)

Distance (mm)	7.5	8.0	8.5	9.0	9.5
Hardness (Hv)	135	132	131	138	160
Estimated strain	5.05	4.66	4.56	5.48	8.69
Thickness (mm)	1.35	1.56	1.69	1.49	0.99

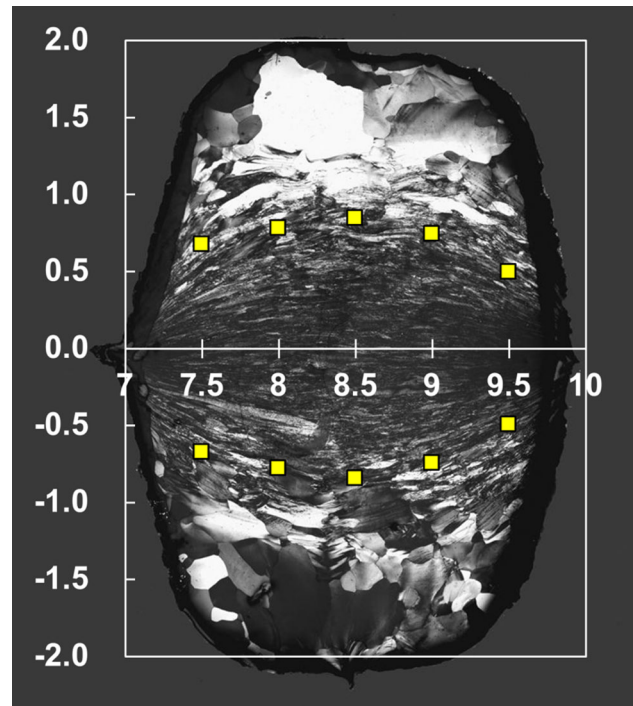


Fig. 14 Positions for thickness values estimated using hardness in Fig. 13 and through Eq. (1) marked in OM image in Fig. 8 after $N = 1/4$

Conclusions

1. Softening occurs in a thicker sample of pure Cu with intense straining by HPT processing and this is probably because of a temperature rise during the processing. No softening occurs in the Al–Mg–Sc alloy.
2. Strained region is localized at the thickness center in both pure Cu and the Al alloy. The width of the intensely strained region increases with the number of revolution and saturates to a width of ~ 2 mm.
3. Preferential straining at the thickness center is not typical behavior of high-purity Al, where softening occurs by intense strain but is common to any type of materials.
4. Equivalent strain in a thick sample imposed by HPT process can be estimated with use of the thickness at the intensely strained region.

Acknowledgements This work was supported in part by the Light Metals Educational Foundation of Japan, in part by a Grant-in-Aid for Scientific Research from the MEXT, Japan, in Innovative Areas “Bulk Nanostructured Metals” (No. 22102004), and in part by a Grant-in-Aid for Scientific Research (S) from the MEXT, Japan (No. 26220909). This study used facilities of severe plastic deformation in the International Research Center on Giant Straining for Advanced Materials (IRC-GSAM) of Kyushu University.

References

- Bridgman PW (1935) Effects of high shearing stress combined with high hydrostatic pressure. *Phys Rev* 48:825–847
- Valiev RZ, Islamgaliev RK, Alexandrov IV (2000) Bulk nanostructured materials from severe plastic deformation. *Prog Mater Sci* 45:103–189
- Valiev RZ, Estrin Y, Horita Z, Langdon TG, Zehetbauer MJ, Zhu YT (2006) Producing bulk ultrafine-grained materials by severe plastic deformation. *JOM* 58(4):33–39
- Zhilyaev AP, Langdon TG (2008) Using high-pressure torsion for metal processing: fundamentals and applications. *Prog Mater Sci* 53:893–979
- Wei Q, Zhang HT, Schuster BE, Ramesh KT, Valiev RZ, Kecskes LJ, Dowding RJ, Magness L, Cho K (2006) Microstructure and mechanical properties of super-strong nanocrystalline tungsten processed by high-pressure torsion. *Acta Mater* 54:4079–4089
- Lee S, Edalati K, Horita Z (2010) Microstructures and mechanical properties of pure V and Mo processed by high-pressure torsion. *Mater Trans* 51:1072–1079
- Korzniok AV, Tram G, Dimitrov O, Korzniokova GF, Idrisova SR, Pakielka Z (2001) The mechanism of nanocrystalline structure formation in Ni₃Al during severe plastic deformation. *Acta Mater* 49:663–671
- Ciuca O, Tsuchiya K, Yokoyama Y, Todaka Y, Umemoto M (2010) Heterogeneous process of disordering and structural refinement in Ni₃Al during severe plastic deformation by high-pressure torsion. *Mater Trans* 51:14–22
- Edalati K, Matsuda J, Arita M, Daio T, Akiba E, Horita Z (2013) Mechanism of activation of TiFe intermetallics for hydrogen storage by severe plastic deformation using high-pressure torsion. *Appl Phys Lett* 103:143902
- Edalati K, Toh S, Ikoma Y, Horita Z (2011) Plastic deformation and allotropic phase transformations in zirconia ceramics during high-pressure torsion. *Scr Mater* 65:974–977
- Levitas VI, Ma Y, Selvi E, Wu J, Patten JA (2012) High-density amorphous phase of silicon carbide obtained under large plastic shear and high pressure. *Phys Rev B* 85:054114
- Edalati K, Horita Z (2010) Application of high-pressure torsion for consolidation of ceramic powders. *Scr Mater* 63:174–177
- Edalati K, Iwaoka H, Toh S, Sasaki K, Horita Z (2013) Application of high-pressure torsion to WC-Co ceramic-based composites for improvement of consolidation, microstructure and hardness. *Mater Trans* 54:1540–1548
- Islamgaliev RK, Kuzel R, Mikov SN, Igo AV, Burianek J, Chmelik F, Valiev RZ (1999) Structure of silicon processed by severe plastic deformation. *Mater Sci Eng A* 266:205–210
- Ikoma Y, Hayano K, Edalati K, Saito K, Guo Q, Horita Z (2012) Phase transformation and nanograin refinement of silicon by processing through high-pressure torsion. *Appl Phys Lett* 101:121908
- Ikoma Y, Hayano K, Edalati K, Saito K, Guo Q, Horita Z, Aoki T, Smith DJ (2014) Fabrication of nanograin silicon by high-pressure torsion. *J Mater Sci* 49:6565–6569. doi:10.1007/s10853-014-8250-z
- Ikoma Y, Ejiri Y, Hayano K, Saito K, Guo Q, Horita Z (2014) Nanograin formation of GaAs by high-pressure torsion. *Philos Mag Lett* 94:1–8
- Harai Y, Ito Y, Horita Z (2008) High-pressure torsion using ring specimens. *Scr Mater* 58:469–472
- Harai Y, Edalati K, Horita Z, Langdon TG (2009) Using ring samples to evaluate the processing characteristics in high-pressure torsion. *Acta Mater* 57:1147–1153
- Sakai G, Nakamura K, Horita Z, Langdon TG (2005) Developing high-pressure torsion for use with bulk samples. *Mater Sci Eng A* 406:268–273
- Yoon SC, Horita Z, Kim HS (2008) Finite element analysis of plastic deformation behavior during high pressure torsion processing. *J Mater Process Technol* 201:32–36
- Hohenwarter A, Bachmaier A, Gludovatz B, Scherlauer S, Pippan R (2009) Technical parameters affecting grain refinement by high pressure torsion. *Int J Mater Res* 100:1653–1661
- Iwaoka H, Harai Y, Horita Z (2010) High-pressure torsion for ring samples in different thicknesses. *Mater Sci Forum* 667–669:51–56
- Iwaoka H, Fujioka T, Harai Y, Horita Z (2011) Development of intense plastic strain and ultrafine grains in thicker samples processed by high-pressure torsion and high-pressure sliding. *J Japan Inst Metals* 75:412–418
- Figueiredo RB, Aguilar MTP, Cetlin PR, Langdon TG (2012) Analysis of plastic flow during high-pressure torsion. *J Mater Sci* 47:7807–7814. doi:10.1007/s10853-012-6506-z
- Song Y, Wang W, Gao D, Kim HS, Yoon EY, Lee DJ, Lee CS, Guo J (2012) Inhomogeneous hardness distribution of high pressure torsion processed IF steel disks. *Mater Sci Appl* 3:234–239
- Hohenwarter A (2015) Incremental high pressure torsion as a novel severe plastic deformation process: processing features and application to copper. *Mater Sci Eng A* 626:80–85
- Ito Y, Horita Z (2009) Microstructural evolution in pure aluminum processed by high-pressure torsion. *Mater Sci Eng A* 503:32–36
- Xu C, Horita Z, Langdon TG (2007) The evolution of homogeneity in processing by high-pressure torsion. *Acta Mater* 55:203–212
- Edalati K, Horita Z (2011) Significance of homologous temperature in softening behavior and grain size of pure metals processed by high-pressure torsion. *Mater Sci Eng A* 528:7514–7523
- Kawasaki M (2014) Different models of hardness evolution in ultrafine-grained materials processed by high-pressure torsion. *J Mater Sci* 49:18–34. doi:10.1007/s10853-013-7687-9
- Edalati K, Fujioka T, Horita Z (2008) Microstructure and mechanical properties of pure Cu processed by high-pressure torsion. *Mater Sci Eng A* 497:168–173
- Sakai G, Horita Z, Langdon TG (2005) Grain refinement and superplasticity in an aluminum alloy processed by high-pressure torsion. *Mater Sci Eng A* 393:344–351
- Horita Z, Langdon TG (2005) Microstructures and microhardness of an aluminum alloy and pure copper after processing by high-pressure torsion. *Mater Sci Eng A* 410–411:422–425
- Kawasaki M, Ahn B, Langdon TG (2010) Effect of strain reversals on the processing of high-purity aluminum by high-pressure torsion. *J Mater Sci* 45:4583–4593. doi:10.1007/s10853-010-4420-9
- Kawasaki M, Figueiredo RB, Langdon TG (2011) An investigation of hardness homogeneity throughout disks processed by high-pressure torsion. *Acta Mater* 59:308–316
- Edalati K, Yamamoto A, Horita Z, Ishihara T (2011) High-pressure torsion of pure magnesium: evolution of mechanical properties, microstructures and hydrogen storage capacity with equivalent strain. *Scr Mater* 64:880–883
- Edalati K, Cubero-Sesin JM, Alhamidi A, Mohamed IF, Horita Z (2014) Influence of severe plastic deformation at cryogenic temperature on grain refinement and softening of pure metals:

- investigation using high-pressure torsion. *Mater Sci Eng A* 613:103–110
39. Edalati K, Horita Z, Furuta T, Kuramoto S (2013) Dynamic recrystallization and recovery during high-pressure torsion: experimental evidence by torque measurement using ring specimens. *Mater Sci Eng A* 559:506–509
40. Edalati K, Ito Y, Suehiro K, Horita Z (2009) Softening of high purity aluminum and copper processed by high pressure torsion. *Int J Mater Res* 100:1668–1673
41. Wetscher F, Vorhauer A, Stock R, Pippan R (2004) Structural refinement of low alloyed steels during severe plastic deformation. *Mater Sci Eng A* 387–389:809–816